Clays and Clay Minerals, Vol. 61, No. 6, 566–579, 2013.

OPEN ACCESS

REDOX CHEMISTRY IN TWO IRON-BENTONITE FIELD EXPERIMENTS AT ÄSPÖ HARD ROCK LABORATORY, SWEDEN: AN XRD AND Fe K-EDGE XANES STUDY

PER DANIEL SVENSSON[1,*] AND STAFFAN HANSEN[2]

[1]Swedish Nuclear Fuel and Waste Management Co, Oskarshamn, Sweden
[2]Centre for Analysis and Synthesis, Department of Chemistry, Lund University, Sweden

Abstract—Excavated bentonite from two large iron–bentonite field experiments at Äspö Hard Rock Laboratory in Sweden was investigated with respect to iron redox chemistry and mineralogy. The iron redox chemistry was studied by Fe K-edge X-ray absorption near edge structure spectroscopy and the mineral phases were studied using X-ray diffraction. Bentonite is to be used as a buffer material in high-level radioactive waste repositories to protect the waste containers from their surroundings. Montmorillonite, which is responsible for the sealing properties in the bentonite, is susceptible to redox reactions. A change in the montmorillonite iron redox chemistry may affect its layer charge and hence its properties. The experiments included are the first Alternative Buffer Material test (ABM1) and the Temperature Buffer Test (TBT). The clays were heated to a maximum of ~130ºC (ABM1) or ~150ºC (TBT) for 2.5 and 7 y, respectively. In the central part of the compacted clay blocks was placed an iron heater and the distance from the heater to the rock was ~10 cm (ABM1) and ~50 cm (TBT), respectively. Eleven different clay materials were included in the ABM1 experiment and five were analyzed here. In the ABM1 experiment, the Fe(II)/Fe(III) ratio was increased in several samples from the vicinity of the heater. Kinetic data were collected and showed that most of the Fe(II)-rich samples oxidized rapidly when exposed to atmospheric oxygen. In the TBT experiment the corrosion products were dominated by Fe(III) and no significant increase in Fe(II) was seen. In ABM1, reducing conditions were achieved, at least in parts of the experiment; in TBT, reducing conditions were not achieved. The difference was attributed to the larger scale of the TBT experiment, providing more oxygen after the installation, and to the longer time taken for water saturation; oxidation of the samples during excavation cannot be ruled out. Minor changes in the bentonite mineral phases were found in some cases where direct contact was made with the iron heater but no significant impact on the bentonite performance in high-level radioactive waste applications was expected as a result.

Key Words—ABM, Alteration, Alternative Buffer Material, Äspö, Bentonite, Iron, Montmorillonite, Redox, Temperature Buffer Test (TBT), XANES, XRD.

INTRODUCTION

The stability of many iron-containing minerals is highly dependent on the oxidation state of the iron and whether the surrounding conditions are oxidizing or reducing. In the Earth's crust the ratio of Fe(III)/Fe(II) is ~0.53, which can be compared to ~1.65 in sediments (Ronov and Yaroshevsky, 1969). The much higher ratio in sediments is related to the instability of the Fe(II) minerals (mainly silicates and sulfides) from the crust under oxygen-rich conditions. Bentonite, a clay that is rich in smectites and formed by the alteration of volcanic ash, has various ratios of divalent and trivalent iron in nature and these are reflected as variations in the color of the bentonite clay from green or blue for divalent iron to grey or red for trivalent iron (*e.g.* bentonite in Bavaria, Germany; South Dakota, USA; Milos, Greece). The dominant smectite in bentonite is montmorillonite and, in montmorillonite, Fe is found together with Al and Mg in the octahedral sheet of the phyllosilicate layer. This Fe is susceptible to redox reactions by chemical or microbiological methods (Pentráková *et al.*, 2013), and if the Fe(III) is reduced to Fe(II) this will impact the layer charge and, hence, many of its important properties also (Stucki *et al.*, 2002). Bentonite processing often involves milling and drying and bentonites are normally investigated and tested after processing and in aerobic conditions, while some applications provide an anaerobic or even reducing environment. One example is engineered barriers for radioactive waste repositories where bentonites are used for their swelling and sealing properties which contribute to the physical and chemical safety functions of the repository. In this application the smectite-rich clay is emplaced at great depth with an oxygen partial pressure which is much lower than at the surface. The deep groundwater is generally anoxic and contains dissolved Fe(II) (Bath and Hermansson, 2009; Grenthe *et al.*, 1992; White and Yee, 1985) and metallic iron present as construction material potentially acts as a reducing agent. Hence, iron–bentonite experiments provide information about the interaction of bentonite with iron, but also provide an opportunity to study the

* E-mail address of corresponding author:
Daniel.Svensson@skb.se
DOI: 10.1346/CCMN.2013.0610609

stability of montmorillonite in reducing conditions. The interaction between metallic iron and bentonite has been studied by several research groups (Guillaume *et al.*, 2004; Lantenois *et al.*, 2005; Charpentiera *et al.*, 2006; Carlson *et al.*, 2007; Perronnet *et al.*, 2008; for a review see Wersin *et al.*, 2008). Potential effects on the bentonite buffer from the corrosion of iron are: (1) reduction of Fe(III) to Fe(II) in montmorillonite potentially affecting the clay-mineral layer charge; (2) dissolution and/or alteration of montmorillonite to another mineral; and (3) cementation of the bentonite by corrosion products affecting the plasticity, hydraulic conductivity, and swelling ability of the clay mineral. Montmorillonite has been found to be either stable or in some cases to convert to Fe-rich trioctahedral smectite, Fe-serpentine, chlorite, vermiculite, or saponite depending on the temperature and experimental conditions.

The present study aimed to investigate the coupled processes of iron redox chemistry and changes in mineralogy in the bentonite buffer in two large-scale field tests at Äspö Hard Rock Laboratory (Alternative buffer material, ABM1; and Temperature Buffer Test, TBT), Sweden, through characterization using X-ray absorption near edge spectroscopy (XANES) and powder X-ray diffraction (XRD). Both field experiments have been analyzed extensively with respect to chemistry, mineralogy, hydromechanical properties, and microbiology (*e.g.* Svensson *et al.* 2011; Åkesson *et al.* 2012). Significant alteration of montmorillonite to non-swelling clay minerals would impact the bentonite buffer performance and, hence, the safety of the high-level radioactive waste repositories. The iron redox chemistry is important when interpreting the experimental conditions, and it is also important that montmorillonite is stable both in oxidizing and reducing environments. The XANES technique has been used successfully in the past to characterize, in a non-destructive way, the oxidation state of iron in various geological, archaeological, and biological samples (Paris *et al.*, 1991; Galoisy *et al.*, 2001; Wilke *et al.*, 2001; Kwiatek *et al.*, 2001; O′Day *et al.*, 2004; Quartieri *et al.*, 2005; Wilke *et al.*, 2005).

EXPERIMENTAL

Alternative Buffer Material experiment (ABM1)

The experiment began at Äspö Hard Rock Laboratory during November 2006 (SKB 2007, p. 281; Svensson *et al.*, 2007, 2011). Three packages were installed. The first, that analyzed here, was excavated in May 2009. The experiment layout (SKB, 2007, p. 281) was similar to the Swedish KBS-3 concept with a metal canister surrounded by clay situated in crystalline bedrock at the ~−450 m level (Figure 1). The differences from the KBS-3 concept were mainly the size, which was smaller (clay-block diameter = 0.3 m; height = 3 m), the central heater consisted of iron rather than copper, and the temperature was 130ºC instead of <100ºC. Eleven different types of clays , *i.e.* with respect to the type of interlayer cations, minerals, and total Fe and smectite content were included in the experiment. For practical reasons not all were analyzed, and among those analyzed not all were investigated to the same extent. The level of monitoring was kept to a minimum to avoid disturbing the experiment. The package was heated from the start and wetted by natural water from cracks in the rock and also artificially by means of an installed wetting system (using natural formation water). The space between the clay blocks and the rock was filled with sand to promote water saturation. After installation, the uppermost part was sealed with bentonite pellets and concrete together with two steel bars to keep the clay blocks in position during consequent swelling of the clay. The Äspö groundwater at the level of the experiment was fairly salty and contained the following approximate molar concentrations of major ions: Na^+, 0.15; Ca^{2+}, 0.15; Mg^{2+}, 0.0002; Cl^-, 0.42; SO_4^{2-}, 0.02 (SKB, 2001).

Temperature Buffer Test experiment (TBT)

The experiment started at Äspö Hard Rock Laboratory in March 2003 at ~−420 m depth (Sandén *et al.*, 2007; Åkesson *et al.* 2012) and was excavated in Spring 2010. The design and size of the TBT experiment was identical to the KBS-3-type installation with the exception that the metal tube was in two parts, made of iron (carbon steel), and the temperature used was up to 150ºC. Compacted ring-shaped blocks (clay-block diameter = 1.8 m) of MX-80 clay were placed around two iron canisters (Figure 1). The hole was 8 m deep. The main objective of the experiment was to improve the general understanding of the thermo-hydromechanical behavior of the bentonite buffer. The water-saturation pressure was controlled by pipes in the sand filling the slot between the bentonite buffer and the rock. The distance from the surface of the canister to the end of the buffer nearest to the surrounding rock was ~0.5 m. Temperature, relative humidity, stress, pore pressure, and total water inflow were monitored during the experiment.

The clays

Five of the 11 clays present in the experiment were chosen (Svensson *et al.* 2011) based on either their potential as suitable buffer materials, their visual appearance at the iron−bentonite interface (*e.g.* Calcigel), or their unusual composition (Callovo-Oxfordian). MX-80 is a natural Na-dominated bentonite from Wyoming, USA, provided by American Colloid Co. Calcigel is the brand name for a natural Ca-dominated bentonite produced as a blend from several Bavarian bentonites by Süd-Chemie AG, Germany. Callovo-Oxfordian is a French sedimentary claystone with very small amounts of smectite and is the host rock for the underground laboratory operated by ANDRA (national radioactive waste-management

https://doi.org/10.1346/CCMN.2013.0610609 Published online by Cambridge University Press

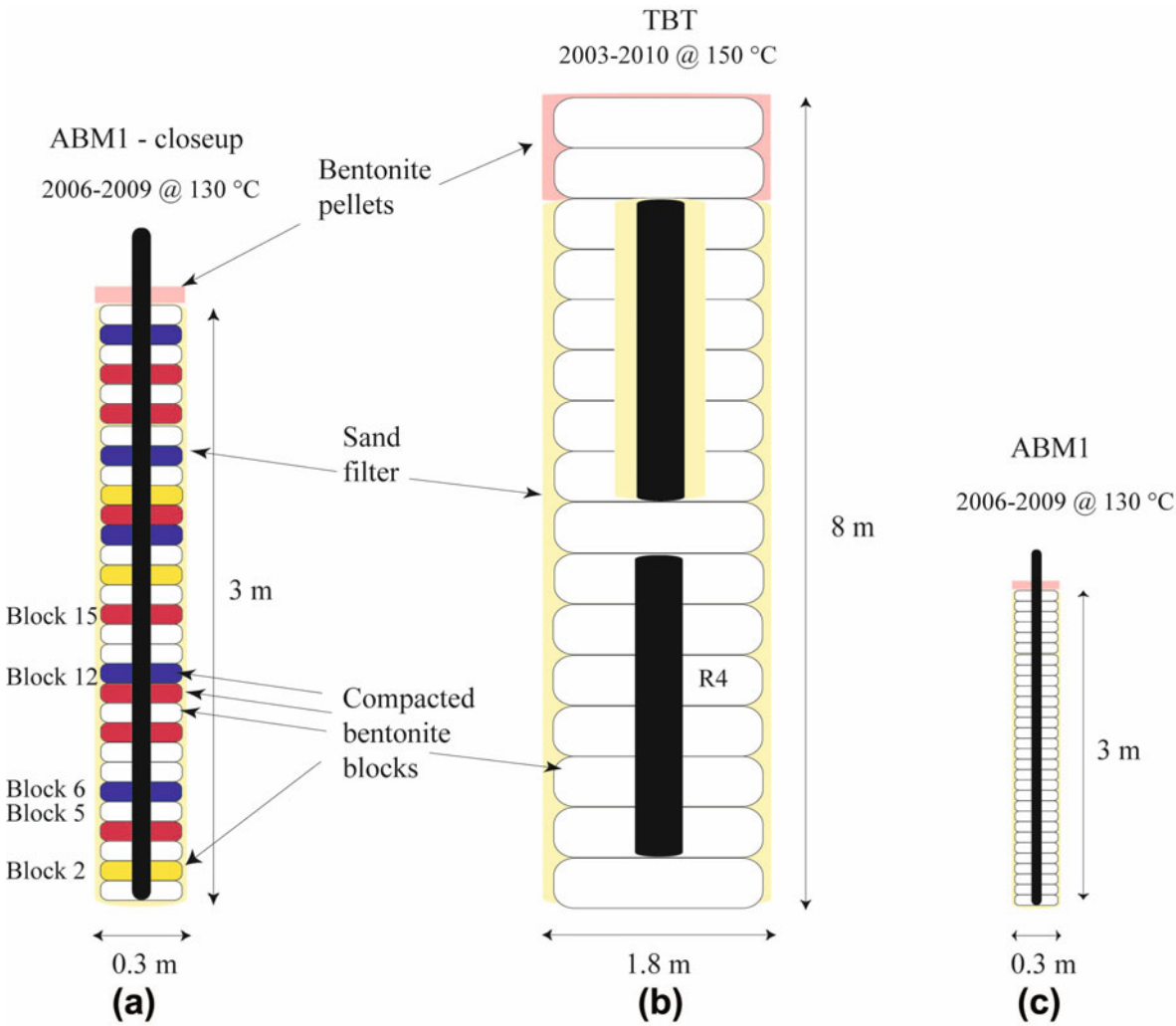

Figure 1. Illustration of the underground field experiments at ~450 m depth in a crystalline rock formation. The locations of the various samples used in this study are marked: (a) ABM1: close-up with detail (several different bentonites); (b) TBT (MX-80 bentonite only); and (c) ABM1 at scale compared to TBT.

agency for France). Deponit CA-N is a commercial Ca-dominated bentonite found at Milos, Greece (produced by the Silver & Baryte Mining Company). Ibeco Seal M-90 is a Na-dominated bentonite from the Republic of Georgia (Svensson *et al.*, 2011).

Elemental analysis and water content

Elemental analysis of the clays was performed by the accredited labs AcmeLabs (Vancouver, Canada) and ALS (Luleå, Sweden) using whole-rock dissolution followed by inductively coupled plasma-atomic emission spectroscopy/mass spectroscopy analysis. The water content was determined gravimetrically, before and after oven drying of the clays at 105ºC for 24 h, by Clay Technology (Lund, Sweden). The saturation was calculated as the amount of water in the sample in relation to the calculated porosity (ratio of the dry bulk density and the grain density).

Excavation and sampling of the field experiments

The excavation of the ABM1 experiment was done by slit drilling of the rock surrounding the package and was combined with wire sawing of the bottom part (Svensson *et al.*, 2010). The entire package was lifted with intact heater-clay-rock interfaces and stored overnight. The rock was removed by combined drilling and chiseling. The surface of the clay blocks was exposed to air as the rock was removed in steps and samples were removed as rapidly as possible and packaged in vacuum-sealed aluminum-polymer bags. The total time used for removal of the rock and packaging was <1 working day and the time from the moment the clay was exposed to ambient atmosphere until the sample was packaged was usually <1 h. Further fine splitting of the samples under atmospheric conditions was performed ~1 week later to create profiles by sawing of specimens ~1 cm × 1 cm × 10 cm in size and again these were stored rapidly

https://doi.org/10.1346/CCMN.2013.0610609 Published online by Cambridge University Press

in vacuum-sealed aluminum-polymer bags. The final sampling was done in inert atmosphere, consisting of either argon in a glove box or a mixture of N_2/H_2 in another glove box with a catalyst. The surface of the samples was removed by scraping using a small, very sharp metal spatula (no metal traces were left on the very soft clay) and the specimens for the XANES measurements were taken from the inner part, parallel to the length of the sample. After ~2 min, the clays in the argon box (O_2 <0.1 ppm, H_2O = 0.6 ppm) showed extensive cracking caused by dehydration of the material (Figure 2), while the samples handled in the H_2+N_2 box showed no tendency to crack due to the greater moisture content in the atmosphere of the box (O_2 < 0.1 ppm, H_2 = 1.2 vol.%, relative humidity 20–30%). The total time between the uptake of the ABM1 package and the first measurement at the synchrotron was 2.5 weeks.

Due to its larger size the TBT experiment was excavated differently. The ring-shaped clay blocks were sampled by consecutive drill-core sampling in the shape of a cross. After the drilling, larger intact sectors of the clay blocks could be sampled. These samples were also packaged in vacuum-sealed aluminum-polymer bags (Åkesson *et al.*, 2012). The final sampling was similar to that for the ABM preparations.

Preparation of the standards and pure montmorillonites

Natural $FeCO_3$ (siderite from Ivigtut, Greenland; Fe(II) in octahedral coordination; freshly ground) was used as the Fe(II) standard and synthetic Fe_2O_3 (Fe(III) in octahedral coordination) was used as the Fe(III) standard. The preparation of the natural Wyoming montmorillonite sample was done by particle-size fractionation (MX-80; <2 μm) and obtained from Clay Technology AB. The reduced montmorillonite was prepared using the citrate-bicarbonate-dithionite (CBD) procedure of Mehra and Jackson (1958). Approximately 100 mg of the purified Na-exchanged clay fraction was used together with 2 g of Na-dithionite (Merck, Germany) added in two steps. The reaction was kept at 80ºC for 4 h, stirred by a magnet, and constantly purged with argon (Strandmøllen, <4.5 ppm O_2). The sample was stored in the centrifuge tube and allowed to dry on a filter paper inside of the glovebox. To check how well these iron phases ($FeCO_3$; Fe_2O_3) work as standards (with respect to the overall shape of spectra) with montmorillonite-rich samples, they were compared qualitatively to natural montmorillonite and to Na-dithionite-reduced Wyoming montmorillonite (Fe(III)- and Fe(II)-dominant, respectively). In order to assure the reliability of the XANES measurements, these standards ($FeCO_3$; Fe_2O_3) were re-measured routinely. As $FeCO_3$ is much more available, stable toward oxygen, and well defined compared to the reduced montmorillonite, $FeCO_3$ and Fe_2O_3 were chosen as the standards to be used.

Figure 2. Calcigel clay (ABM1). The dark area to the right is 1 cm × 1 cm in size and was in contact with the heater. The cracking was caused by the low humidity in the argon glove box.

XANES – data collection

The samples were mounted between sulfur-free XRF tapes (TF-500, FLUXANA GmbH & Co. KG, Bedburg-Hau, Germany; to avoid effects on the measurement) in a polypropylene sample holder. The sample holder was 1 mm thick and the X-ray beam was of the order of 0.5 mm × 0.5 mm in size. X-ray absorption data were recorded at beam line I811 at the MAX-lab synchrotron, Lund University, Sweden. The beamline is based on a super-conducting multi-pole wiggler that provides a high-flux X-ray beam. The design is based on vertical collimation of the beam by a cylindrical mirror before a double-crystal monochromator in Si(111) direction (~0.7 eV in energy resolution). The second crystal is bendable for horizontal focusing, and vertical focusing on the sample is achieved by means of a second cylindrical mirror. The horizontal focus is obtained by sagittal bending of the second monochromator crystal (Carlson *et al.*, 2006). Three consecutive scans were recorded over the range −150 to +500 eV (relative to the absorption edge) and merged and analyzed as an average unless otherwise stated. The scans were of 'quickscan' type (~2200 steps in ~120 s; 0.33 eV step size). The 'quickscan' mode was chosen because the reproducibility of the measurement was of much greater importance than the signal/noise ratio, and as the 'quickscan' was done much more quickly (~3 min compared to 1 h for normal scans), it allowed for more measurements and more samples within the limited time at the beamline. The faster measuring time of the 'quickscan' also minimized the risk of sample oxidation and allowed for kinetic studies. The Lytle detector was used (fluorescence mode) due to the rather low Fe content in some of the clays. Metallic iron foil was used for energy calibration, and a manganese filter was added to remove X-rays with lower energies.

XANES – data evaluation

The free software *Athena* (version 0.8.059; Bruce Ravel, Brookhaven National Laboratory, USA) was

https://doi.org/10.1346/CCMN.2013.0610609 Published online by Cambridge University Press

used. *Athena* is a graphical front end to *IFEFFIT* (version 1.2.5; Matt Newville, Consortium for Advanced Radiation Sources, University of Chicago, USA). The first inflection point of the iron foil was adjusted to 7112.0 eV. The data were normalized in three steps: (1) The spectral region from −150 to −30 eV was fitted to a pre-edge straight line which was subtracted from the data; (2) a post-edge straight line was fitted to the spectral region from +150 to ~+400 eV which was subtracted from the data; and (3) an average value of an interval in the post-edge range was used for scaling the data to achieve a step height of unity at the absorption edge. Due to the long spectral region before and after the K edge, the automatic normalization routine of the software worked well in all cases. Semi-quantitative determination of the Fe(II) content was achieved by linear combination fitting of standards in the *Athena* software, using the default interval of −20 to +30 eV relative to the absorption edge. The strategy was to carry out the linear-combination fit in an interval as small as possible and as close to the edge as possible to exclude or minimize the effect from the differences in the absorption spectra in the pre- and post-edge regions. A smaller interval (−4 to +2 eV) was also evaluated for the quantification but had negligible effect on the result.

X-ray diffraction

Powder XRD data were collected at beam-line I711 at the MAX-lab synchrotron, Lund University, Sweden (Cerenius *et al.*, 2000) using a Mar system with a flat CCD detector (Mar 165, 2048 × 2048 pixels). The X-ray beam had a wavelength of 0.994 Å, as refined using a LaB_6 reference sample, and was 0.9 mm × 0.9 mm in size. Data were collected for a period of 30 s. The data were evaluated using the software *Fit2d* (version V12.077, A.P. Hammersley, ESRF, France). The sampling was carried out in ambient atmosphere. A capillary was filled with ground clay and sealed with modeling clay. The samples used were, thus, essentially unoriented and oxidized.

RESULTS AND DISCUSSION

Below, the Fe(II) contents refer to the Fe(II)/Fe-total ratio. The data points are the result of the evaluation of three consecutive measurements that were merged. To investigate the statistical variation in the Fe(II) determinations the individual scans were also evaluated in the Callovo-Oxfordian clay (Table 1).

XANES – standards ($FeCO_3$, Fe_2O_3)

The edge of the $FeCO_3$ was situated at lower energies compared to the edge of the Fe_2O_3 (Figure 3). In the spectral region at energies greater than the edge, the shapes of the spectra were rather different, reflecting the differences in crystal structure between the two compounds (Wilke *et al.*, 2001). The natural and the reduced montmorillonite showed a shift

Table 1. Statistical-error calculations for the Callovo-Oxfordian (COX) clay comparing three analyses in the same point on the sample with measurements made at different points of the sample.

Sample	Measurement no	Fe(II)/Fe total	Average (std. dev.)
COX	1	34.2	33.2 (1.6)
32 mm from heater	2	31.3	
	3	34.0	
COX	1	32.9	33.6 (2.4)
52 mm from heater	2	31.6	
	3	36.2	
COX	1	30.1	31.0 (0.90)
67 mm from heater	2	31.1	
	3	31.8	
COX	1	28.3	27.2 (1.7)
90 mm from heater	2	25.2	
	3	28.1	
	Total average (std. dev.)	31.0 (3.0)	
COX original clay sample 1	1	41.6	39.7 (1.7)
	2	38.6	
	3	38.9	
COX original clay sample 2	1	38.9	40.6 (1.5)
	2	41.6	
	3	41.4	
COX original clay sample 3	1	49.1	48.1 (0.92)
	2	47.3	
	3	47.9	
	Total average (std. dev.)	43.0 (4.2)	

https://doi.org/10.1346/CCMN.2013.0610609 Published online by Cambridge University Press

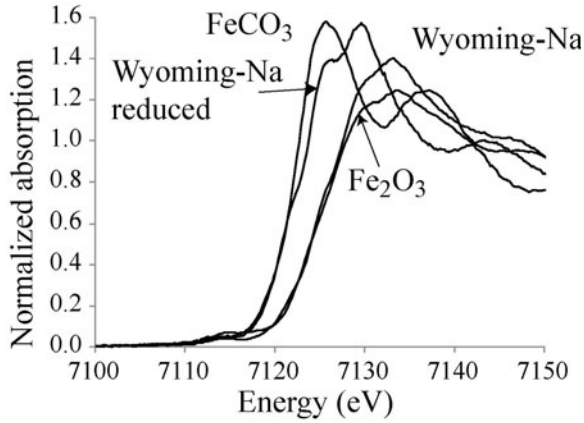

Figure 3. XANES spectra of the standards compared to natural and artificially reduced Wyoming MX-80 montmorillonite (Na dithionite).

in energy of the edge, however, but only minor differences in the features of the spectra were noted. The edges of the natural Wyoming montmorillonite (MX-Na) and the ferric oxide overlapped, indicating that Fe(III) was dominant in the non-reduced montmorillonite (Figure 3). The reduced montmorillonite (MX-Na-reduced) and the ferrous carbonate also overlapped, indicating that Fe(II) was dominant in the reduced montmorillonite (the overlap decreased somewhat at higher energies in the absorption edge). The curvature of the spectra of the iron standards were rather similar to those of the montmorillonites in the energy interval close to the absorption edge (no sharp, intense, white lines *etc*.), which was the interval used for the quantifications. Hence, Fe_2O_3 and $FeCO_3$ were agreed as suitable standards, at least for the semi-quantitative work needed in the present study. In general, the amount of Fe(II) was greater while using the montmorillonite standards than when the iron compounds were used, however. This either indicated that (1) the reduced montmorillonite was not 100% Fe(II) or (2) the structural differences, as well as potential matrix effects, influenced the shape of the curve and, hence, also the quantification. The absolute value of the Fe(II)/Fe(III) ratio was, thus, somewhat sensitive to the standards used, though the relative trends were insensitive to them.

Bentonite iron redox chemistry in ABM1 and TBT

MX-80 (ABM1, block 2). The innermost sample (0.5 mm from the central heater) showed a low-energy shoulder at the edge, similar to but smaller than that in the reduced MX-Na-montmorillonite (Figure 4a). The samples at 0.5 to 8.5 mm from the iron heater showed a significant increase in Fe(II) (41−50% of the total iron; Figure 4b**)** compared to the original material (with ~10% Fe(II)). The Fe content approximately doubled close to the heater (8 wt.% Fe_2O_3) compared to the reference material at 4 wt.%. The block was fully water saturated.

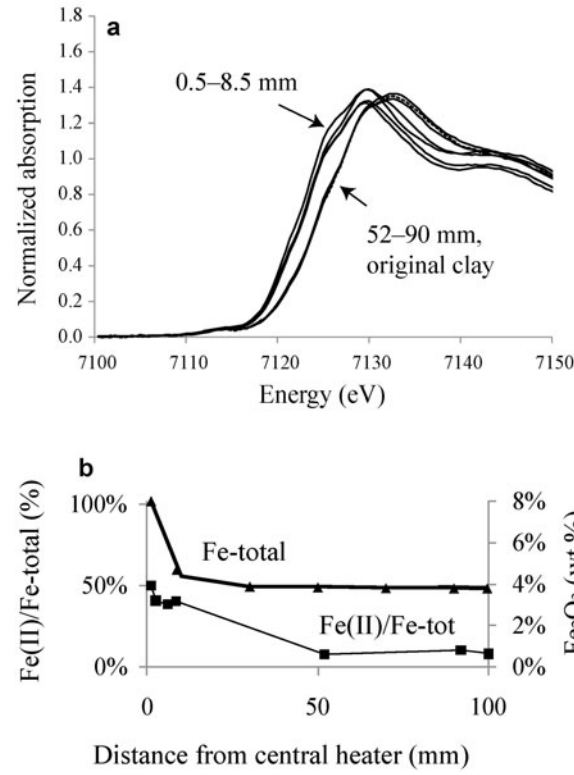

Figure 4. ABM1 MX-80. (a) XANES spectra of the samples and original clay (dashed line). (b) Fe(II) (squares) and Fe_2O_3 (triangles) content in the block. The reference value of the original clay is located at 100 mm in the Figure.

*Calcigel (ABM1, block 5).*The two innermost samples had adsorption edges lower in energy than the rest, and the Fe(II) contents were 39% and 43% for the 0.5 and 2.5 mm samples, respectively (Figure 5). The samples at between 8 and 90 mm and the original sample were internally very similar and dominated by Fe(III). Again, the total amount of Fe was observed to roughly double close to the central heating element (11 wt.% Fe_2O_3 in the closest sample and 5% in the original material). The block was fully water saturated.

Callovo-Oxfordian (ABM1, block 12). Due to loss of material, no measurements could be performed on samples close to the iron heater for this material. The absorption edge of the original clay was situated at lower energy compared to all of the sampled points (Figure 6a), meaning that the Fe(II) content was somewhat greater before the experiment than after. The Fe(II) content in the samples at 32 mm, 52 mm, 67 mm, and 90 mm were 37, 32, 28, and 27%, respectively, while the original clay was 42−48% (Figure 6b). As no obvious trend in the Fe(II) content could be seen within this ABM1 sample, it was chosen for statistical evaluation. In Table 1, the statistical variation in the Fe(II) content in a specific point (measured three times) was compared to the variation between different points on the sample. The standard

https://doi.org/10.1346/CCMN.2013.0610609 Published online by Cambridge University Press

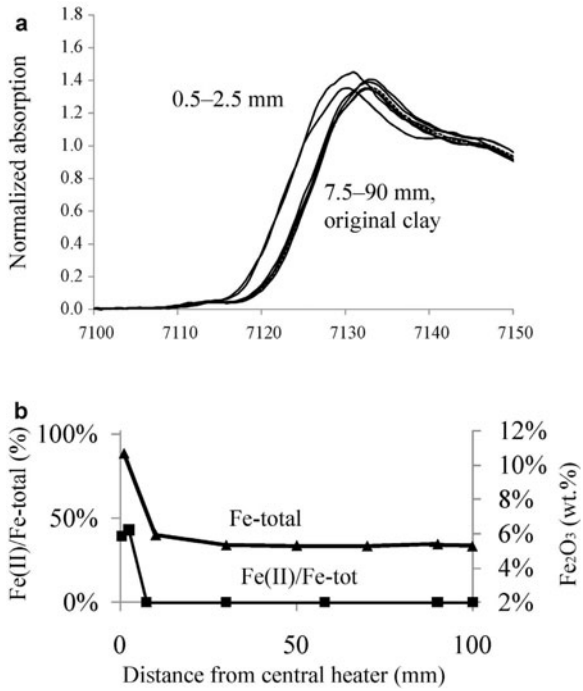

Figure 5. ABM1 Calcigel. (a) XANES spectra of the samples and original clay (dashed line). (b) Fe(II) (squares) and Fe_2O_3 (triangles) content in the block. The reference value of the original clay is located at 100 mm in the Figure.

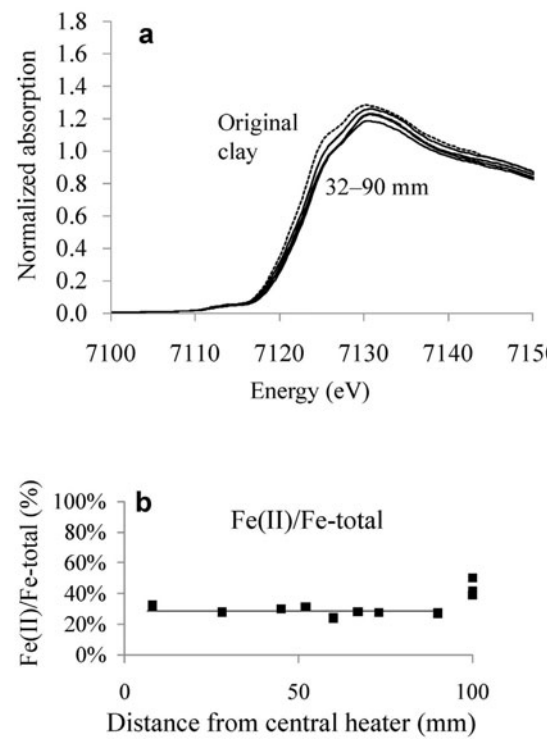

Figure 6. ABM1 Callovo-Oxfordian. (a) XANES spectra of the samples and original clay (dashed line). (b) Fe(II) (squares) content in the block. The reference value of the original clay is located at 100 mm in the Figure.

deviation due to the inhomogeneity of the clay was 1.3−4.5 times greater than the variation in the repeated X-ray absorption measurements. These results indicated that the main fluctuation in this type of measurement was caused by the use of a small probe (0.5 mm × 0.5 mm) and the sample not being completely homogenous. The average Fe(II) content of the excavated material was 31% (std. dev. 3.0%) and for the references it was 43% (std. dev. 4.2%); hence the excavated material had a smaller Fe(II) content than the original clay. This could be explained by oxidation of the Fe(II) minerals originally present in the clay by the oxygen in the air before anaerobic conditions were achieved. One such reaction is oxidation of pyrite which has been identified previously in this type of clay (*e.g.* Gaucher *et al.*, 2009). The original clay had an Fe content of 5.4 wt.% Fe_2O_3, and the block was fully water saturated.

Deponit CA-N (ABM1, block 15). In the Deponit CA-N clay, all the samples deviated little from the original clay that was dominated by trivalent iron. The samples closest to the iron heater (0.5 and 6 mm) showed a slight increase in Fe(II) (changed from ~0 to 5%). A minor increase in total Fe toward the iron canister was noted (5.1 wt.% Fe_2O_3 compared to 4.6 wt.% in the original clay). The block was fully water saturated.

IbecoSeal M-90 (ABM1, block 6). The Fe(II) contents of the three innermost samples (0.5−24 mm) increased to 21, 9, and 4 wt.%, respectively, compared to the original clay at 0 wt.%. The original clay had an Fe content of 3.8 wt.% Fe_2O_3. The block was fully water saturated.

Kinetic oxidation experiments

Samples that were rich in Fe(II) were later exposed to ambient atmospheric oxygen. The oxidation of Fe(II) to Fe(III) was followed *in situ* over time. The purpose of the dynamic experiments was to establish the sensitivity of the samples to oxidation, in order to obtain input data for the design of future sample-handling procedures and also potential diagnostic information about the nature of the Fe(II) compounds present. The existence of oxygen-sensitive phases is evidence for anoxic conditions.

Several of the Fe(II)-rich samples from the ABM1 package, *e.g.* MX-80 (2.5 and 6 mm samples), exhibited substantial oxidation in air (Figure 7a,b). The two innermost Fe(II)-rich samples of the Calcigel clay (0.5 and 6 mm samples) exhibited substantial differences in oxidation behavior (Figure 7c,d). The 0.5 mm sample was only somewhat oxidized from 36 to 33% in 50 min (Figure 7c), implying the presence of a compound stable under atmospheric oxygen, *e.g.* magnetite or a combination of siderite and Fe(III) phases such as montmorillonite, hematite, or goethite. None of these suggested new phases was confirmed by XRD, however. The Fe(II) content in the 6 mm sample decreased from 23 to 3%

https://doi.org/10.1346/CCMN.2013.0610609 Published online by Cambridge University Press

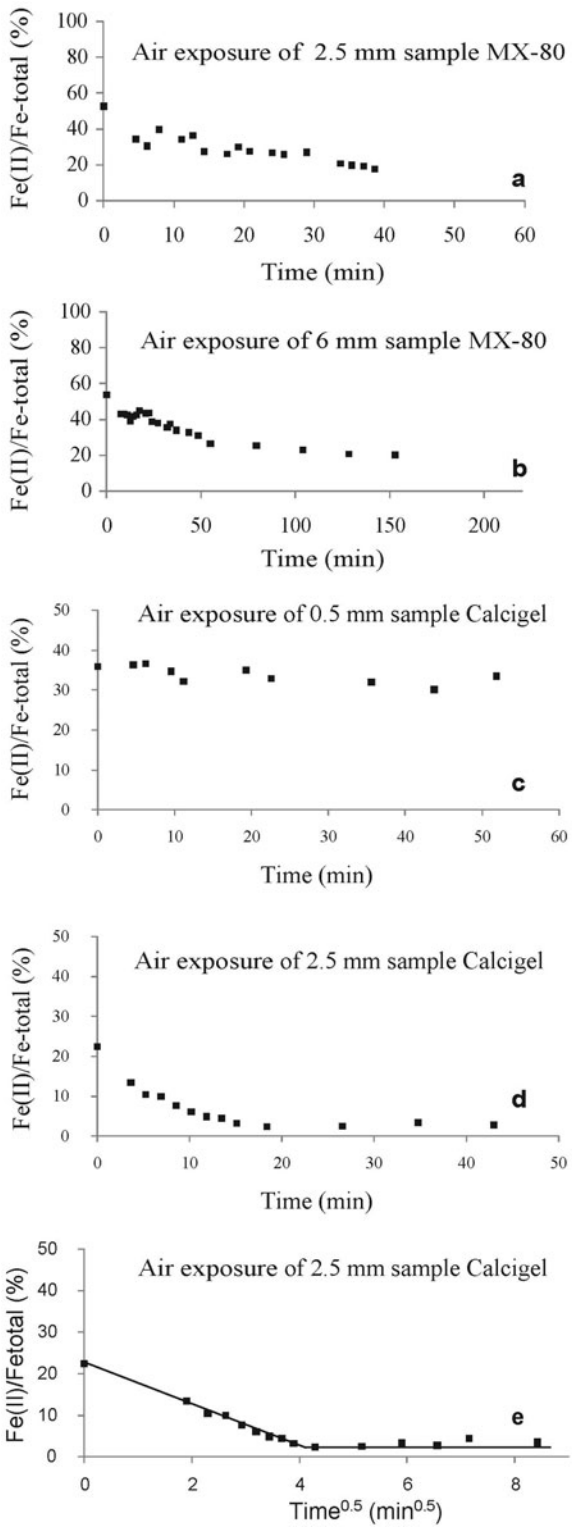

Figure 7. Oxidation of Fe(II)-rich samples from ABM1 in air, with time (analyzed by XANES). Distances given are from the central iron heater.

over 20 min. When the Fe(II) content was plotted *vs*. the square root of time, a linear relation was found (Figure 7e; R^2 = 0.99). This is typical of a diffusion-controlled process (Crank, 1980) such as drying of the clay followed by in-diffusion of air within the porous clay structure. This implies the presence of reduced montmorillonite, green rust, or any other oxygen-sensitive Fe(II) phase in both MX-80 and the Calcigel clays. The oxygen-sensitive Fe(II) phases in MX-80 did not follow a similar oxidation curve to that of Calcigel (linearity toward the square root of time) probably because of the sample preparation, as the particle size and cracks affects the drying mechanisms of the clay (*e.g.* a non-uniform distribution of small and large particles would give oxidation curves initially dominated by the smaller particles as they oxidize more quickly, and in the end dominated by the larger grains).

MX-80 (TBT, sample R4:0-302)

Nine samples were taken over the interval 0.5–541 mm from the central heater. All samples had X-ray absorption curves with shapes similar to those of the original clay (Figure 8a). Most samples were very close to the original clay curve in terms of energy, with some scattering (Figure 8b). The Fe(II) contents were in the range 14–24%. The average Fe(II) content of all the samples was 15%, which is somewhat larger than the original clay, at 11%. Observation of a small increase in the Fe(II) content in the TBT experiment was also confirmed by research at Åbo University, Finland, using Mössbauer spectroscopy (Åkesson *et al*., 2012), though that team concluded that the increase was too small to be detected reliably with that method. In contrast, the 2.5 and 4 mm samples were Fe(III)-dominant, with an Fe(II) content of 0–5% (Figure 8b). This increase in Fe(III) was attributed to small magnetic particles that could be separated from the innermost sample and this corrosion product was dominated entirely by Fe(III) according to XANES (Figure 8c). The magnetic Fe(III) particles were brownish-black and were identified (using XRD) as maghemite (reference data ICSD 98-007-9196). The total iron profile indicated an almost two-fold increase in Fe content close to the heater (7 wt.% Fe_2O_3) compared to the original clay material (4 wt.%; Figure 8b). The block was ~90% saturated toward the canister and fully saturated toward the rock.

In a bentonite subject to redox reactions, circumstances were complicated by the presence of varying proportions of Fe-containing phases of different chemical nature (silicates, oxides, hydroxides, sulfides, *etc*.) with divalent or trivalent Fe in tetrahedral or octahedral coordination. An increase in Fe(II) content is, therefore, far from trivial to locate to a specific phase. Reducing conditions were reached in parts of the ABM1 experiment as several samples were high in Fe(II) and also sensitive to oxidation when exposed to air. In the TBT experiment the conditions were the opposite. Little or no

https://doi.org/10.1346/CCMN.2013.0610609 Published online by Cambridge University Press

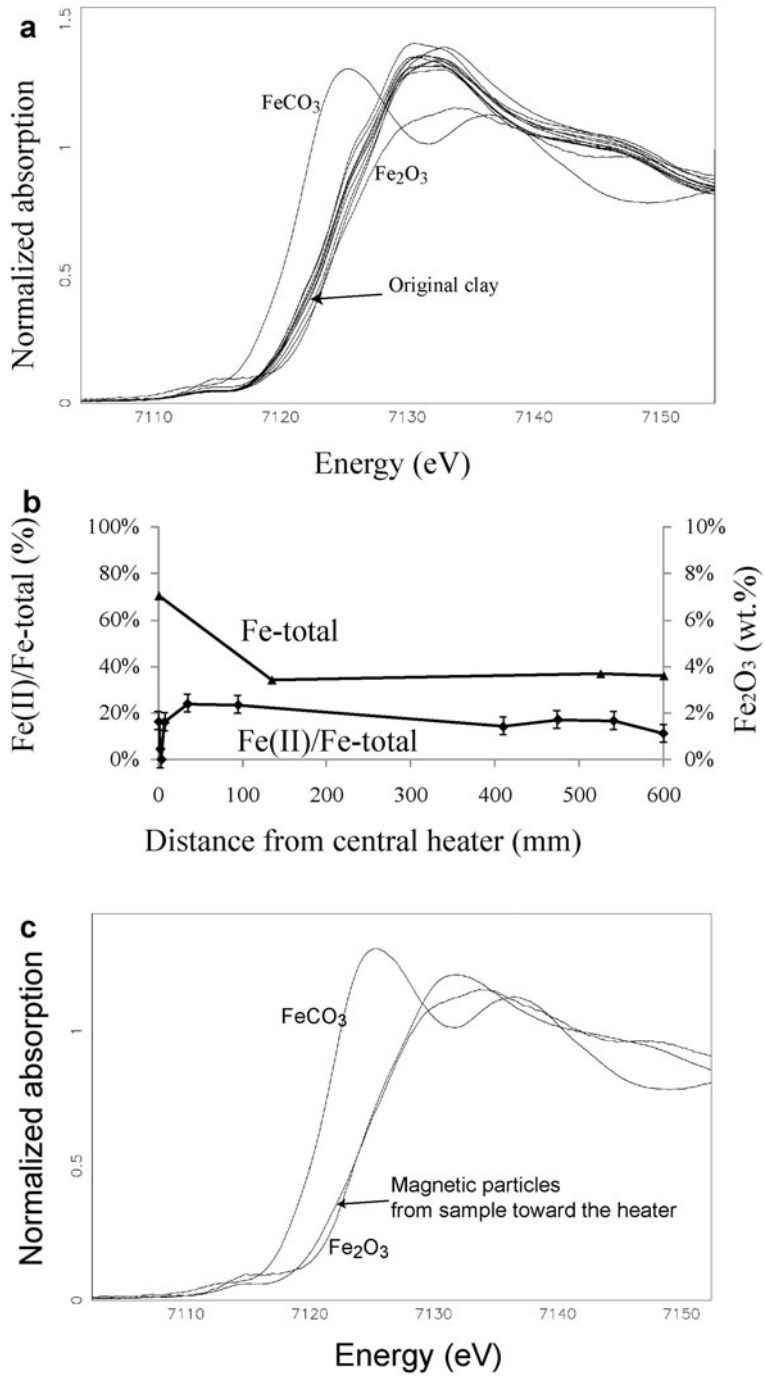

Figure 8. TBT MX-80. (a) XANES spectra of the samples and original clay (dashed line). (b) Fe(II) and Fe_2O_3 content in the block. The reference value of the original clay is at 600 mm. (c) XANES spectrum of separated magnetic particles from the bentonite–canister interface compared to the Fe(II) and Fe(III) references.

increase in Fe(II) was observed in the bentonite buffer, and the only corrosion product isolated was dominated by Fe(III). The ABM1 experiment probably reached anoxic or reducing conditions, while in the TBT experiment oxic conditions prevailed. Two main differences between the experiments were the larger size and higher temperature of the TBT experiment (Figure 1). The thickness of the bentonite buffer in the TBT experiment was five times greater than the ABM1 buffer (50 cm *vs*. 10 cm). In terms of diffusion-controlled transport, this means that roughly $5^2 = 25$ times longer was required for complete water saturation due to the

https://doi.org/10.1346/CCMN.2013.0610609 Published online by Cambridge University Press

larger size (Crank, 1980). Water saturation would continue until all porous space in the deposition hole was filled with water and bentonite; then the swelling pressure would increase and, at a certain point, cause further water flow to cease (defined as 100% saturation). The longer water-saturation period also delayed the iron-corrosion processes that were important consumers of the available oxygen. The larger size also introduced more trapped air, so more oxygen existed in the experiment as the bentonite pore volume was much larger. The water saturation was complete in all ABM1 samples, while the TBT clay was fully saturated only at the contact with the rock and the degree of saturation then decreased to ~90% at the contact with the heater. As iron corrosion consumes oxygen, corresponding experiments with copper and bentonite are likely to become anoxic over even longer time periods, as copper consumes oxygen much more slowly.

The aerobic oxidation of pyrite and siderite is expected to be a rapid process while the oxidation of Fe(II)-containing silicates and the diffusion of O_2 into the surrounding, anaerobic rock is expected to be much slower (Bath and Hermansson, 2009). The time estimated for restoring anaerobic conditions varies for different areas in the KBS-3 type repository, *i.e.* the wetted bentonite buffer, <300 y (Wersin *et al.*, 1994); the saturated tunnel backfill (bentonite and crushed rock), <1 month (Grandia *et al.*, 2006); and the water-filled cracks in the surrounding granitic rock, <1 week (SKB, 2001).

Bentonite mineral-phase transformations in ABM1 and TBT

Minor changes were found in the powder XRD patterns. The basal spacing of the MX-80 montmorillonite (d_{001}) was greater in the excavated material than in the original clay (in both the ABM1 and TBT experiments, Figure 9a,b). This is compatible with a partial ion exchange from Na to Ca, which was expected after contact with the Ca-rich Äspö groundwater (Table 1). The explanation for the increase in basal spacing is that Ca-montmorillonite has two water layers and a basal spacing of ~15 Å at 30–50% relative humidity (similar to ambient drying conditions), while Na-montmorillonite has only one water layer at this relative humidity, at ~12 Å. In the Calcigel clay (Figure 9c) the opposite occurred; some Ca was exchanged for Na and the basal spacing decreased somewhat (the Calcigel started with greater Ca levels than that corresponding to equilibrium in the Äspö groundwater). These ion-exchange reactions were also confirmed by chemical extraction using alcoholic solutions of NH_4Cl (Svensson *et al.* 2011) and by Cu-triethylenetetramine cation exchange (Dohrmann *et al.* 2013). No corrosion products were identified in the XRD patterns, indicating that the corrosion products were unstable, amorphous, very poorly crystalline, or present at very low levels. The system is very complex and many intermediate phases may form making the formation of the thermodynamically stable compound very slow (Ardizzone and Formaro, 1982).

The position of the 060 reflection (Figure 9; close-up) distinguishes a dioctahedral clay mineral from a trioctahedral one; changes in the position are, therefore, an indicator of chemical changes in the silicate sheet. The innermost TBT MX-80 sample showed a somewhat changed appearance in the 060 region with a new broad reflection at ~38º (Figure 9b close-up, corresponding to ~1.50 to 1.55 Å). A similar change was also seen in the innermost Calcigel sample (block #15; Figure 9c close-up). However, no significant change was observed in the ABM MX-80 0.5 mm sample (block # 2; Figure 9a close-up). These changes are signs of the formation of small amounts of a trioctahedral smectite in direct contact with the iron heater. The amount of cristobalite (reflection at 14.2°) was reduced slightly in the innermost ABM1 MX-80 sample (0.5 mm from canister) and it was even more reduced in the innermost TBT MX-80 sample (0.5 mm) in relation to the intensity of the montmorillonite 4.48 Å reflection.

The formation of trioctahedral smectite and the decrease in the amount of cristobalite in the vicinity of the corroding iron has also been noted by other groups working with similar samples in both ABM (Kaufhold *et al.*, 2013) and in TBT (Åkesson *et al.*, 2012). Early results from the ABM2 experiment (6.5 y old experiment excavated in 2013) have confirmed the presence of a newly formed trioctahedral clay phase and the dissolution of cristobalite, and the extent of formation was much greater than for the shorter ABM1 experiment (Svensson, 2013). Changes in MX-80 (block #11), though not in Calcigel (#23), were identified by Kaufhold *et al.* (2013). The formation of trioctahedral smectite may, thus, not only depend on the type of bentonite but also on the position of the bentonite block within the experiment. The cristobalite may have been dissolved by the combination of heat and the alkaline environment created by the corroding iron, beneficial for silicate dissolution. The dissolved silica may then have reacted with other ions present (such as Ca^{2+}, Mg^{2+}, and Fe^{2+}) and formed the observed trioctahedral smectite mineral. An increase in total MgO has been correlated to the trioctahedral smectite (Kaufhold *et al.* 2013), suggesting that the smectite mineral is probably a Mg- and/or Fe(II)-dominated trioctahedral smectite mineral such as saponite, stevensite, or ferrosaponite, as neither the Mg nor Fe has been assigned to any other crystalline phase. Stevensite, which is a trioctahedral smectite, has been synthesized by hydrothermal reaction of amorphous silica and $MgCO_3$ at basic conditions and 100ºC in 0.5–20 h (Ogawa *et al.*, 1991). Formation from cristobalite and available Mg^{2+}, instead of from the alteration of montmorillonite, should also be considered as a possible route.

https://doi.org/10.1346/CCMN.2013.0610609 Published online by Cambridge University Press

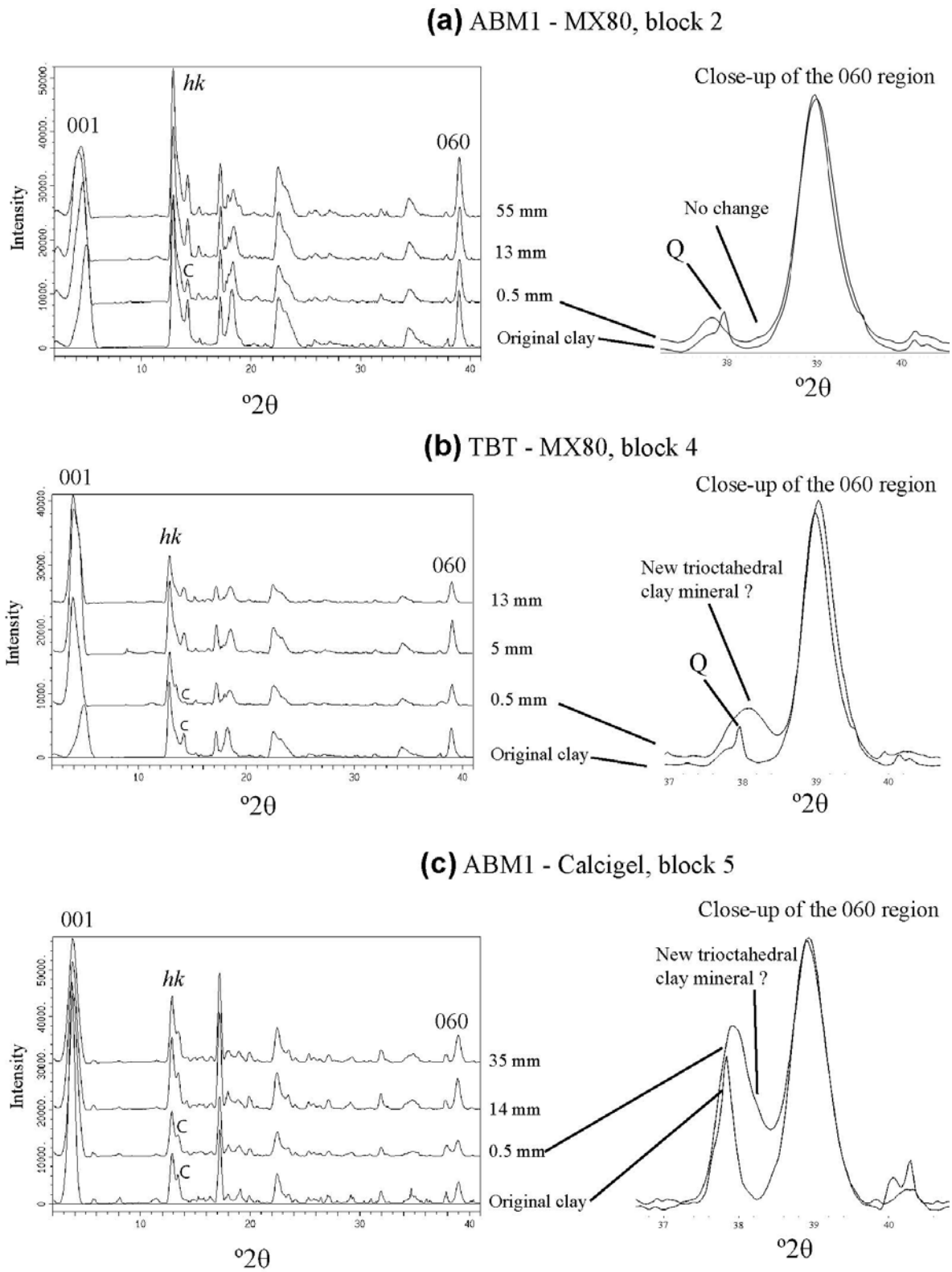

Figure 9. XRD patterns of (a) MX-80 (ABM1), (b) MX-80 (TBT), and (c) Calcigel (ABM1) with distances from the heater, compared to the original clays. C = cristobalite and Q = quartz.

https://doi.org/10.1346/CCMN.2013.0610609 Published online by Cambridge University Press

The observations are similar to those described previously from similar experiments with compacted bentonite. An increase in Fe(II)/Fe-total from 36 to 75% and total Fe increase from 3 to 13 wt.% was noted by Carlson *et al.* (2007) using Mössbauer spectroscopy (compacted MX-80 bentonite with carbon steel wires and coupons; 50ºC; 2.5 y). An Fe(II) increase from 50 to 60% (Mössbauer spectroscopy) and from 20 to 35% (XANES), and total iron from 3 to ~20 wt.% (compacted MX-80; 8 years; 20ºC) was identified by Kumpulainen *et al.* (2010). Compacted MX-80 (90ºC; 8 months) in contact with an iron bar was used by Martin *et al.* (2008). The surface of the bar was passivated by the formation of magnetite and siderite (according to Raman spectroscopy and SEM-EDX analysis), though the montmorillonite was unaffected by the experiment. The results from these experiments with compacted bentonite are all fairly similar. Several bentonites were investigated with XRD and no evidence of significant montmorillonite alteration could be identified in any of them, except from minor formation of a trioctahedral smectite at the iron interface. The cation exchange capacity (CEC, determined using the Cu-triethylenetetramine method of Meier and Kahr, 1999) was more or less unaffected: ABM1 MX-80 (block 2) – 86 (original clay 84 meq/100 g) and ABM1 Calcigel (block 5) – 67 (original clay 64 meq/100 g) (Svensson *et al.*, 2011); in TBT MX-80 – 85 (original clay 83 meq/100 g; Åkesson *et al.*, 2012). This was somewhat surprising, as the CEC was expected to decrease due to the dilution of the corrosion products formed. This supports the hypothesis that the trioctahedral smectite, which contributes to the CEC, may have formed from sources other than montmorillonite. No signs of change in swelling behavior in XRD data of oriented clay fractions were observed (TBT experiment; Mg-saturated; <0.5 μm fraction; ethylene glycol-saturated, Åkesson *et al.*, 2012).

In contrast, in several studies performed with a very high liquid/solid ratio, extensive smectite alteration was observed. Guillaume *et al.* (2004) found that at 80 to 150ºC saponite was formed, whereas at 300ºC the product was chlorite. The bentonite–iron interaction under similar but alkaline conditions were studied by Charpentiera *et al.* (2006). In the 80 and 150ºC experiments, montmorillonite remained as the predominant clay mineral, though at 300ºC vermiculite was formed, together with a trioctahedral Fe-rich smectite. The transformation of MX-80 bentonite and iron powder in a thermal gradient from 80 to 300ºC was investigated by Jodin-Caumon *et al.* (2010). Smectite was found to convert to Fe-rich trioctahedral smectite, Fe-serpentine, and chlorite depending on the temperature. These investigators all used liquid/solid mass ratios of 10. An experiment with an even greater liquid/solid mass ratio of 16, using an original clay consisting of both montmorillonite and kaolinite, was carried out by Perronet *et al.* (2008) who identified the neoformation of Fe-rich clay minerals (7 Å phase).

The density and/or liquid/solid ratio together with the temperature and pH seem to be important when predicting the outcome of an iron-bentonite experiment; the same conclusion was reached by Mosser-Ruck *et al*. (2010). In compacted bentonite only interlayer water was present, while in dilute experiments external bulk water was also available. In the compacted system, gradients may appear, while at high liquid/solid ratio the system is more homogenous. The presence of large amounts of external bulk water probably increased the possibility of dissolution of smectite. The more the experiments mimic the true technical application the more the results can be used in relation to the application. All technical bentonite buffers in high-level radioactive waste repositories are of compacted bentonite with a low liquid/solid ratio. Depending on the technical setup, however, the expected temperature may be either high or low. If a high-level nuclear waste canister of iron is in contact with bentonite, the reaction will take place at high temperature (~90ºC or higher). If the iron is inside a copper canister as in the Swedish KBS-3 concept, however, the iron and bentonite will come into contact at a much later stage, at which point the temperature will be much lower, probably equivalent or close to the temperature of the host rock (~5–10ºC). In the Swedish KBS-3H concept of SKB the plan is to emplace the canisters horizontally (in contrast to the reference setup KBS-3 which has the canisters in vertical orientation) in packages containing both the canister and the bentonite buffer rings. The packages will be held together in a super-container made of iron or other metallic material. In this case the iron–bentonite reaction will take place at an intermediate temperature close to the rock surface. At the rock surface the iron is also much less protected than inside the bentonite, near sulfides in the groundwater. The interaction between construction iron in the rock and backfill bentonite in the tunnels will also occur at low temperature, equivalent or close to the temperature of the host rock. The main conclusion is that in all the studies discussed, including the present one, no significant montmorillonite alteration was found in experiments involving compacted bentonite.

Consequences for bentonite buffer used in high-level nuclear waste storage

In the ABM1 experiment, reducing conditions were achieved, at least in parts of the experiment, while in the TBT experiment they were not. Oxidation of the samples during excavation cannot be ruled out, however. The impact on buffer performance should probably be further evaluated if the Fe(II) increase cannot be attributed to a phase other than montmorillonite. No significant montmorillonite alteration was observed in any case. In the vicinity of the corroding iron metal, an increase in total iron content and Fe(II)/Fe-total was seen, as well as minor formation of what could be a trioctahedral smectite mineral and a minor decrease in the cristobalite content. The trioctahedral smectite may either be formed

https://doi.org/10.1346/CCMN.2013.0610609 Published online by Cambridge University Press

from exchangeable interlayer Mg^{2+} or Fe(II) from corrosion and dissolved cristobalite, or formed as an alteration product from montmorillonite. As the total amount of the triocthedral smectite formed is very small and as the properties of the trioctahedral smectite were probably similar to those of montmorillonite, no significant change in the performance would be expected at this level of transformation. Further investigation of more samples from future ABM excavations are needed in order to separate true differences between the bentonites from incidental differences due to experimental conditions.

ACKNOWLEDGMENTS

Financial support by the Swedish Nuclear Fuel and Waste Management Co (SKB) is gratefully acknowledged. Ola Karnland, Clay Technology AB, Lund, is acknowledged for stimulating discussions. Ulf Nilsson and Torbjörn Sandén (also Clay Technology) are acknowledged for help with sample handling and glove-box work. Mattias Åkesson, Clay Technology AB, Lund, is acknowledged for providing the TBT samples and information regarding the experiment, and ANDRA, France, for jointly running the experiment.

REFERENCES

Ardizzone, S. and Formaro, L. (1982) Temperature induced phase transformation of metastable $Fe(OH)_3$ in the presence of ferrous ions. *Materials Chemistry and Physics*, **8**, 125–133.

Åkesson, M., Olsson, S., Dueck, A., Nilsson, U., and Karnland, O. (2012) TBT – Hydro-mechanical and chemical/mineralogical characterizations. SKB Report, P-12-06, SKB, Stockholm.

Bath, A. and Hermansson, H.-P. (2009) Biogeochemistry of redox at repository depth and implications for the canister. Swedish Radiation Safety Authority, Report 2009: 28.

Carlson, L., Karnland, O., Oversby, V.M., Rance, A.P., Smart, N.R., Snellman, M., Vähänen, M., and Werme, L.O. (2007) Experimental studies of the interactions between anaerobically corroding iron and bentonite. *Physics and Chemistry of the Earth*, **32**, 334–345.

Carlson, S., Clausén, M., Gridneva, L., Sommarin, B., and Svensson, C. (2006) XAFS experiments at beamline I811, MAX-lab synchrotron source, Sweden. *Journal of Synchrotron Radiation*, **13**, 359–364.

Cerenius, Y., Ståhl, K., Svensson, L.A., Ursby, T., Oskarsson, Å., Albertsson, J., and Liljas, A., (2000) The crystallography beamline I711 at MAX II. *Journal of Synchrotron Radiation*, **7**, 203.

Charpentiera, D., Devineau, K., Mosser-Ruck, R., Cathelineau, M., and Villiéras, F. (2006) Bentonite-iron interactions under alkaline condition: An experimental approach. *Applied Clay Science*, **32**, 1–13.

Crank, J. (1980) *The Mathematics of Diffusion*, 2nd edition, Clarendon Press, Oxford.

Dohrmann, R., Olsson, S., Kaufhold, S., and Sellin, P. (2013) Mineralogical investigations of the first package of the alternative buffer material test II. Exchangeable cation population rearrangement. *Clay Minerals*, **48**, 215–233.

Galoisy, L., Calas, G., and Arrio, M.A. (2001) High-resolution XANES spectra of iron in minerals and glasses: structural information from the pre-edge region. *Chemical Geology*, **174**, 307–319.

Gaucher, E.C., Tournassat, C., Pearson, F.J., Blanc P., Crouzet, C., Lerouge, C., and Altmann, S. (2009) A robust model for pore-water chemistry of clayrock. *Geochimica et Cosmochimica Acta*, **73**, 6470–6487.

Grandia, F., Domènech, C., Arcos, D., and Duro, L. (2006) Assessment of the oxygen consumption in the backfill. Geochemical modelling in a saturated backfill. SKB Report, R-06-106, SKB, Stockholm.

Grenthe, I., Stumm, W., Laaksuharju, M., Nilsson, A.-C., and Wikberg, P. (1992) Redox potentials and redox reactions in deep groundwater systems. *Chemical Geology*, **98**, 131–150.

Guillaume, D., Neaman, A., Cathelineau, M., Mosser-Ruck, R., Peiffert, C., Abdelmoula, M., Dubessy, J., Villiéras, F., and Michau, N. (2004) Experimental study of the transformation of smectite at 80 and 300ºC in the presence of Fe oxides. *Clay Minerals*, **39**, 17–34.

Jodin-Caumon, M.C., Mosser-Ruck, R., Rousset, D., Randi, A., Cathelineau, M., and Michau, N. (2010) Effect of a thermal gradient of iron-clay interactions. *Clays and Clay Minerals*, **58**, 667–681.

Kaufhold, S., Dohrmann, R., Sandén, T., Sellin, P., and Svensson, D. (2013) Mineralogical investigations of the alternative buffer material test – I. Alteration of bentonites. *Clay Minerals*, **48**, 199–213.

Kumpulainen, S., Kiviranta, L., Carlsson, T., Muurinen, A., Svensson, D., Sasamoto, H., and Wersin, P. (2010) Long-term alteration of bentonite in the presence of metallic iron. SKB Report, R-10-52, SKB, Stockholm.

Kwiatek, W.M., Galka, M., Hanson, A.L., Paluszkiewicz, C., and Cichocki, T. (2001) XANES as a tool for iron oxidation state determination in tissues. *Journal of Alloys and Compounds*, **328**, 276–282.

Lantenois, S., Lanson, B., Muller, F., Bauer, A., Jullien, M., and Plançon, A. (2005) Experimental study of smectite interaction with metal Fe at low temperature: 1. Smectite destabilization. *Clays and Clay Minerals*, **53**, 597–612.

Martin, F.A., Bataillon, C., and Schlegel, M.L. (2008) Corrosion of iron and low alloyed steel within a water saturated brick of clay under anaerobic deep geological disposal conditions: An integrated experiment. *Journal of Nuclear Materials*, **379**, 80–90.

Mehra, O.P. and Jackson, M.L. (1958) Iron oxide removal from soils and clays by a dithionite citrate system buffered with sodium bicarbonate. *Clays and Clay Minerals*, **7**, 317–327.

Meier, L.P. and Kahr, G. (1999) Determination of the cation exchange capacity (CEC) of clay minerals using complexes of copper(II) ion with triethylenetetramine and tetraethylenepentamine. *Clays and Clay Minerals*, **47**, 386–388.

Mosser-Ruck, R., Cathelineau, M., Guillaume, D., Charpentiera, D., Rousset, D., Barres, O., and Michaue, N. (2010) Effects of temperature, pH, and iron/clay and liquid/clay ratios on experimental conversion of dioctahedral smectite to berthierine, chlorite, vermiculite, or saponite. *Clays and Clay Minerals*, **58**, 280–291.

O'Day, P.A., Rivera Jr., N., Root, R., and Carroll S.A. (2004) X-ray absorption spectroscopic study of Fe reference compounds for the analysis of natural sediments. *American Mineralogist*, **89**, 572–585.

Ogawa, M., Sato, T., Takahashi, N., and Tanaka, M. (1991) Synthetic stevensite and process for preparation thereof. U.S. Patent 5,004,716 A, filed April 2, 1990, and published April 2, 1991.

Paris, E., Mottana, A., and Mattias, P. (1991) Iron environment in a montmorillonite from Gola del Furlo (Marche, Italy). A synchrotron radiation XANES and a Mössbauer study. *Mineralogy and Petrology*, **45**, 105–117.

Pentráková, L., Su, K., Pentrák, M., and Stucki, J. W. (2013) A

review of microbial redox interactions with structural Fe in clay minerals. *Clay Minerals*, **48**, 543–560.

Perronnet, M., Jullien, M., Villiéras, F., Raynal, J., Bonnin, D., and Bruno, G. (2008) Evidence of a critical content in Fe(0) on FoCa7 bentonite reactivity at 80°C. *Applied Clay Science*, **38**, 187–202.

Quartieri, S., Riccardi, M.P., Messiga, B., and Boscherini, F. (2005) The ancient glass production of the medieval Val Gargassa glasshouse: Fe and Mn XANES study. *Journal of Non-Crystalline Solids*, **351**, 3013–3022.

Ronov, A.B. and Yaroshevsky, A.A. (1969) Chemical composition of the Earth′s crust. Pp 37–57 in: *The Earth's Crust and Upper Mantle* (I. Hart, editor). Geophysical Monograph, **13**, American Geophysical Union, Washington, DC.

Sandén, T., Goudarzi, R., Combarieu, M. Åkesson, M., and Hökmark, H. (2007) Temperature buffer test – design, instrumentation and measurements. *Physics and Chemistry of the Earth*, **32**, 77–92.

SKB (2001) O_2 depletion in granitic media. The REX project. SKB Technical Report, TR-01-05, SKB, Stockholm.

SKB (2007) RD & D Programme. Programme for research, development and demonstration of methods for the management and disposal of nuclear waste. SKB Technical Report, TR-07-12, SKB, Stockholm.

Stucki, J.W., Lee, K., Zhang, L., and Larson, R.A. (2002) Effects of iron oxidation state on the surface and structural properties of smectites. *Pure and Applied Chemistry*, **74**, 2081–2094.

Svensson, D. (2013) Early observations in a large scale 6½ year iron-bentonite field experiment (ABM2) at Äspö hard rock laboratory, Sweden. Conference abstract, 50th annual meeting of The Clay Minerals Society. October 6–10, Urbana-Champaign, Illinois, USA.

Svensson, D., Eng, A., and Sellin, P. (2007) Alternative buffer material experiment. Conference abstract, 3rd International meeting, Clays in natural & engineered barriers for radioactive waste confinement, September 17–18, Lille, France.

Svensson, D., Sandén, T., Kaufhold, S., and Sellin, P. (2010) Alternative buffer material experiment – experimental concept and progress. Conference abstract, 4th International meeting, Clays in natural & engineered barriers for radioactive waste confinement. March 29–April 1, Nantes, France.

Svensson, D., Dueck, A., Nilsson, U., Olsson, S., Sandén, T., Eriksson, S., Jägervall, S., and Hansen, S. (2011) Alternative Buffer Material. Status of the ongoing laboratory investigation of reference materials and test package 1. SKB Technical Report, TR-11-06, SKB, Stockholm

Wersin, P., Spahiu, K., and Bruno, J. (1994) Time evolution of dissolved oxygen and redox conditions in a HLW repository. SKB Technical Report, TR-94-02, SKB, Stockholm.

Wersin, P., Birgersson, M., Olsson, S., Karnland, O., and Snellman, M. (2008) Impact of corrosion-derived iron on the bentonite buffer within the KBS-3H disposal concept. The Olkiluoto site as case study. SKB Report, R-08-34, SKB, Stockholm.

White, A.F. and Yee, A. (1985) Aqueous oxidation-reduction kinetics associated with coupled electron-cation transfer from iron-containing silicates at 25°C. *Geochimica et Cosmochimica Acta*, **49**, 1263–1275.

Wilke, M., Farges, F., Petit, P.-E., Brown Jr., G.E., and Martin, F. (2001) Oxidation state and coordination of Fe in minerals: An Fe K-XANES spectroscopic study. *American Mineralogist*, **86**, 714–730.

Wilke, M., Partzsch, G.M., Bernhardt, R., and Lattard, D. (2005) Determination of the iron oxidation state in basaltic glasses using XANES at the K-edge. *Chemical Geology*, **220**, 143–161.

(*Received 29 November 2012; revised 2 December 2013; Ms. 731; AE: E. Ferrage*)